The molecular basis for T-type Ca^{2+} channel inhibition by G protein $\beta_2\gamma_2$ subunits

Seth D. DePuy*, Junlan Yao*, Changlong Hu*, William McIntire*, Isabelle Bidaud†, Philippe Lory†, Fraydoon Rastinejad*, Carlos Gonzalez‡, James C. Garrison*, and Paula Q. Barrett*§

Departments of *Pharmacology and ‡Molecular Physiology and Biological Physics, University of Virginia, Charlottesville, VA 22908; and †Département de Physiologie, Institut de Génomique Fonctionnelle, Centre National de la Recherche Scientifique, Unité Mixte de Recherche 5203, Institut National de la Santé et de la Recherche Médicale U661, Université Montpellier I et II, 34095 Montpellier, France

Edited by David E. Clapham, Harvard Medical School, Boston, MA, and approved August 1, 2006 (received for review May 12, 2006)

Gβγ, a ubiquitous second messenger, relays external signals from G protein-coupled receptors to networks of intracellular effectors, including voltage-dependent calcium channels. Unlike high-voltage-activated Ca^{2+} channels, the inhibition of low-voltage-activated Ca^{2+} channels is subtype-dependent and mediated selectively by $G\beta_2$-containing dimers. Yet, the molecular basis for this exquisite selectivity remains unknown. Here, we used pure recombinant Gβγ subunits to establish that the $G\beta_2\gamma_2$ dimer can selectively reconstitute the inhibition of α_{1H} channels in isolated membrane patches. This inhibition is the result of a reduction in channel open probability that is not accompanied by a change in channel expression or an alteration in active-channel gating. By exchanging residues between the active $G\beta_2$ subunit and the inactive $G\beta_1$ subunit, we identified a cluster of amino acids that functionally distinguish $G\beta_2$ from other Gβ subunits. These amino acids on the β-torus identify a region that is distinct from those regions that contact the Gα subunit or other effectors.

α-1H channels | channel regulation | Gβγ dimers

Low-voltage-activated (LVA) Ca^{2+} currents carried by α_{1H} Ca^{2+} channels play well documented roles in the regulation of neuronal excitability (1). α_{1H} currents are important in the perception and transmission of noxious stimuli (2) and in the development of neuropathic pain after peripheral axonal injury (3), and the α_{1H} gene (*CACNA1H*) is a susceptibility locus for childhood absence epilepsy (4). α_{1H} channels are regulated by kinases (5), redox potential (6), and the activation of G protein-coupled receptors that generate membrane-delimited signals (7–9). For example, in neurons of the dorsal root ganglion, $GABA_B$ (10), adenosine A1 (11), and dopamine (7) receptor activation produce a steady-state inhibition of α_{1H} whole-cell currents. Current inhibition is reproduced by photoreleased GTPγS and blocked by pertussis toxin pretreatment (10) and can be voltage-independent. Thus, dopamine-mediated inhibition is not temporarily reversed by a strong depolarizing pulse and is replicated in excised membrane patches, manifesting as a decrease in the probability of opening of LVA α_{1H} channels (7). Analogously, $G\beta_2\gamma_2$ dimers elicit a voltage-independent inhibition of α_{1H} whole-cell currents carried by recombinant channels by binding directly to the II-III loop of the channel protein (9).

To date, 7 Gβ and 12 Gγ subunits have been identified in mammalian systems, producing a large number of potentially unique dimers that could differ in their interactions among effectors (12). However, the complexity of these signals is mitigated by the reality that the $G\beta_{1-4}$ subunits are >85% identical in amino acid sequence (13). Thus, although there are differences in potency and efficacy, Gβγ dimers containing any of the $G\beta_{1-4}$ subunits can regulate many effectors, such as G protein-activated inwardly rectifying K (GIRK) K^+ channels (13, 14) and high-voltage-activated Ca^{2+} channels (15–18). In surprising contrast, only Gβγ dimers containing $G\beta_2$ decrease whole-cell currents carried by recombinant α_{1H} channels; dimeric isoforms containing $G\beta_{(1,3-4)}$ are not modulatory (9).

In this study, we took advantage of this remarkable differential modulation to understand how this selectivity in Gβ signaling is achieved. Our results identify a cluster of amino acids that functionally distinguish $G\beta_2$ from other Gβ subunits and define a region that is distinct from those regions on the β-torus that make contact with the α-subunit or other effectors.

Results

$G\beta_2$-containing dimers selectively inhibit the activity of α_{1H} channels and do not inhibit the α_{1G} channel, a T-type Ca^{2+} channel homolog (9). Because the II-III loop of α_{1H} channels preferentially binds $G\beta_2$-containing subunits and confers current inhibition to unregulated α_{1G} channels (9), we hypothesized that modulation of α_{1H} channel gating by $G\beta_2\gamma_2$ was mediated by the direct binding of Gβγ dimers to the channel protein and, thus, would be membrane-delimited. To test this possibility, we measured single-channel currents in membrane patches excised from HEK-293 cells stably expressing α_{1H} Ca^{2+} channels, comparing the effects of pure, recombinant $G\beta_2\gamma_2$ and $G\beta_1\gamma_2$ dimers (Fig. 1). I_{Ca} was activated by a depolarizing pulse to −35 mV, and control activity was monitored for 5–6 min before direct application of either Gβγ isoform. α_{1H} Ca^{2+} channels active at −35 mV displayed diverse patterns of small openings (Fig. 1 *A* and *B*) and full steady-state potential-dependent inactivation (data not shown). After the application of $G\beta_2\gamma_2$ to the bath ($\bar{x}$ = 2 nM), α_{1H} channels opened less frequently, decreasing the average ensemble current (105 sweeps, concatenated from three cells) to 45.7% of control (Fig. 1*A*). By contrast, bath application of $G\beta_1\gamma_2$ ($\bar{x}$ = 2 nM) did not change the frequency of single-channel opening or decrease the average ensemble current (Fig. 1*B*).

Fig. 1*C* illustrates the time course of channel modulation by $G\beta_2\gamma_2$ from an exemplar recording of an excised patch with at least two active α_{1H} channels. For each sweep, a value of channel open probability (NP_o) was calculated from the ratio of the total open time and the test pulse duration. $G\beta_2\gamma_2$ markedly decreased NP_o and concomitantly increased the number of silent sweeps (denoted by a solid circle, Fig. 1*C*). The decrease in NP_o ranged from 72% to 27% in seven patches and was accompanied by a 181 ± 57% increase in the number of null sweeps (Fig. 1*D*). This degree of inhibition was close to maximal, because a 10-fold-higher concentration of $G\beta_2\gamma_2$ ($\bar{x}$ = 20 nM) only de-

Author contributions: S.D.D., P.L., and P.Q.B. designed research; S.D.D., C.H., and I.B. performed research; J.Y., W.M., F.R., and C.G. contributed new reagents/analytic tools; S.D.D. and P.Q.B. analyzed data; and J.C.G. and P.Q.B. wrote the paper.

The authors declare no conflict of interest.

This paper was submitted directly (Track II) to the PNAS office.

Abbreviations: GIRK, G protein-activated inwardly rectifying K; HA, hemagglutinin; LVA, low-voltage-activated; NP_o, channel open probability.

§To whom correspondence should be addressed at: Department of Pharmacology, University of Virginia School of Medicine, 1300 Jefferson Park Avenue, Charlottesville, VA 22908. E-mail: pqb4b@virginia.edu.

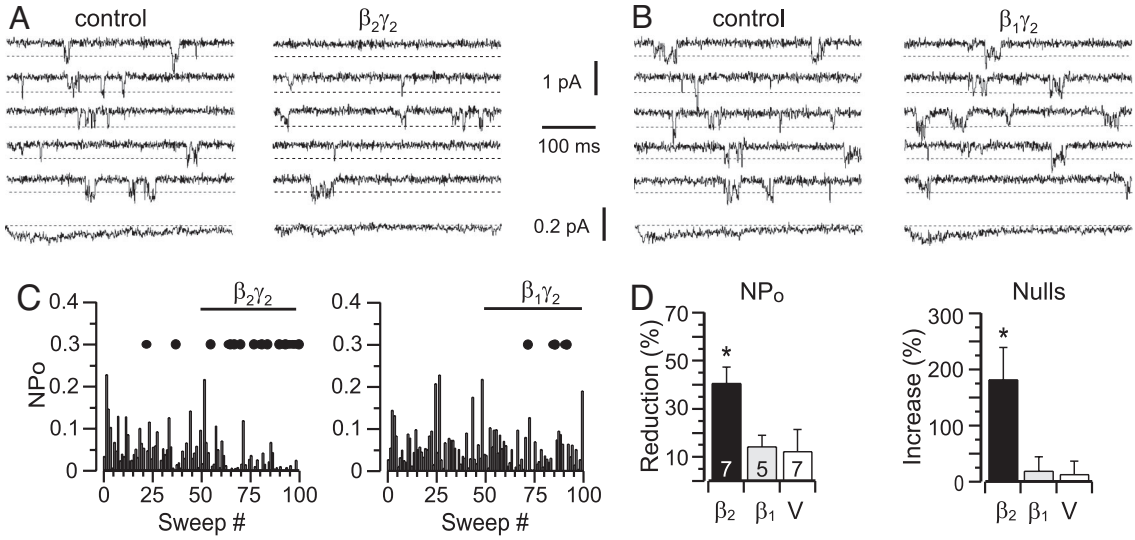

Fig. 1. Recombinant G$\beta_2\gamma_2$, but not G$\beta_1\gamma_2$, inhibits α_{1H} channel activity in patches excised from HEK-293 cells. (*A* and *B*) Shown are records and analysis of single-channel I_{Ca} currents elicited by repeated (6-sec) test pulses to −35 mV from −90 mV. Five consecutive sweeps and the ensemble average of 105 sweeps concatenated from three cells (bottom trace) recorded before (*Left*) and after (*Right*) reconstitution of 1 nM G$\beta_2\gamma_2$ (*A*) or G$\beta_1\gamma_2$ (*B*) into the patch. (*C*) Time course of NP_o from two representative patches before and after adding G$\beta\gamma$. Sequential exposure to vehicle (sweeps 1–50) and in sweeps 51–100 G$\beta\gamma$ dimer: G$\beta_2\gamma_2$ (*Left*) or G$\beta_1\gamma_2$ (*Right*). Blank/inactive sweeps (Nulls) are indicated by filled circles arbitrarily drawn at 0.3 (NP_o) for clarity. (*D*) Bar graphs plot mean ± SEM of the percent reduction in NP_o (*Left*) or percent increase in nulls (*Right*) elicited by G$\beta_2\gamma_2$ or G$\beta_1\gamma_2$ relative to vehicle exposure for each patch. Numbers are patches recorded for each condition. *, $P < 0.05$ compares vehicle with treatment groups by ANOVA.

creased NP_o to 70.9 ± 7.6% ($n = 3$). Moreover, the G$\beta_2\gamma_2$-induced decrease in NP_o was not accompanied by an increase in the latency to first opening (49.7 ± 4.3 ms (control), 48.7 ± 5.8 ms ($\beta_2\gamma_2$), $n = 3$ cells, not significant) or by a change in the single-channel conductance of 6.4 pS (Fig. 5*C*, which is published as supporting information on the PNAS web site). The amplitude distribution of the test-pulse currents before and after the addition of G$\beta_2\gamma_2$ yielded average midpoints for the primary conductance state (70% of openings) that were not different from each other (−0.419 ± 0.003 pA (vehicle); −0.389 ± 0.004 pA ($\beta_2\gamma_2$), at −35 mV). Nor did G$\beta_2\gamma_2$ alter the open-state distribution of dwell times, which remained well fitted to the sum of two exponentials with unchanged proportions ($\tau_1 = 0.44 \pm 0.07$ ms (68%); $\tau_2 = 2.86 \pm 0.15$ ms (32%), Fig. 5 *A* and *B*). Therefore, a G$\beta_2\gamma_2$-elicited decrease in α_{1H} whole-cell current is the apparent consequence of a decrease in the number of channel openings. By contrast, G$\beta_1\gamma_2$ ($\bar{x} = 2$ nM) had no effect on NP_o in five patches showing macroscopic currents (Fig. 1*B* and *D*), consistent with its failure to modulate whole-cell current in published overexpression studies (9). Finally, we tested for the ability of G$\beta_2\gamma_2$ to inhibit $\alpha_{1H}(G_{II-III})$ unitary currents. In concert with its whole-cell behavior, G$\beta_2\gamma_2$ failed to decrease the open probability of $\alpha_{1H}(G_{II-III})$ chimeric channels (117 ± 13%, $n = 4$) in which the II-III loop is replaced with that from unregulated α_{1G} channels (9). Taken together, these data, with recombinant protein delivered at low nanomolar concentrations, establish a modulation that is membrane-delimited, and selective for Gβ_2, and clarify the elementary events underlying the G$\beta_2\gamma_2$-elicited inhibition of whole-cell current. This modulation differs fundamentally from the inhibition of N-, P/Q-, and R-type Ca^{2+} channels that is mediated by all G$\beta\gamma$ subtypes (13, 17, 19).

Because of the difficulty of obtaining patches expressing a single recombinant channel, our analysis of single-channel currents precluded a distinction between a G$\beta_2\gamma_2$-mediated change in N, the number of active channels, and P_o, the probability of finding the channel open. Therefore, we used nonstationary noise analysis to analyze the fluctuations in macroscopic current caused by the opening and closing of α_{1H} channels to determine and compare the effect of G$\beta_2\gamma_2$ with that of G$\beta_1\gamma_2$ (20, 21). We conducted variance analysis of the current elicited upon repolarization to −70 mV after a test pulse to +30 mV that was optimized to produce maximal channel opening with no apparent macroscopic inactivation. Fitted parameters from variance-mean current plots (Fig. 2 *A–C*), indicate no change in single-channel current current (i) or the maximal activity (P_o^{max}) of an active channel but rather, a G$\beta_x\gamma_2$-elicited change in the number (N) of active channels in the membrane. Notably, the expression of G$\beta_1\gamma_2$ increased the number of active channels in the membrane, in contrast to G$\beta_2\gamma_2$, which reduced it.

Because cell-surface biotinylation experiments (9) suggested that G$\beta_2\gamma_2$ did not reduce the surface expression of α_{1H} channels, we interpreted the G$\beta_2\gamma_2$-elicited decrease in active channel number (N) to be the result of reduced channel activity. To verify this interpretation, we used an α_{1H} channel construct that incorporates a hemagglutinin (HA) epitope on the large extracellular loop of domain I (S5-H5). We evaluated surface expression of channels, using luminometry to monitor the levels of chemiluminescence (22). α_{1H}-HA channels are fully functional and, like wild-type channels, are modulated by G$\beta_2\gamma_2$ (58.3 ± 7.4% inhibition at −20 mV, $n = 12$). Although the expression of the Gγ_2 subunit alone did not affect the membrane expression of α_{1H}-HA channels, coexpression with either Gβ_1 or Gβ_2 significantly increased the membrane expression of channels [45 ± 3.2% of control (G$\beta_1\gamma_2$, $n = 54$) and 59 ± 4.8% of control (G$\beta_2\gamma_2$, $n = 53$); Fig. 2*D*]. These data likely explain the G$\beta_1\gamma_2$-elicited increase in active channel number revealed with noise analysis but cannot account for the reduction in functional channel number mediated by G$\beta_2\gamma_2$. Thus, we conclude that G$\beta_2\gamma_2$ markedly decreases α_{1H} channel NP_o solely by diminishing the stochastic behavior of α_{1H} channels.

The Gβ subunit is a member of a large family of proteins that share a highly conserved WD40 repeating motif. In the Gβ subunit, the seven repeating motifs define a circular propeller-like structure, with each "blade" formed by four antiparallel β-strands designated a–d (13). Extensive mutational analysis has

NEUROSCIENCE

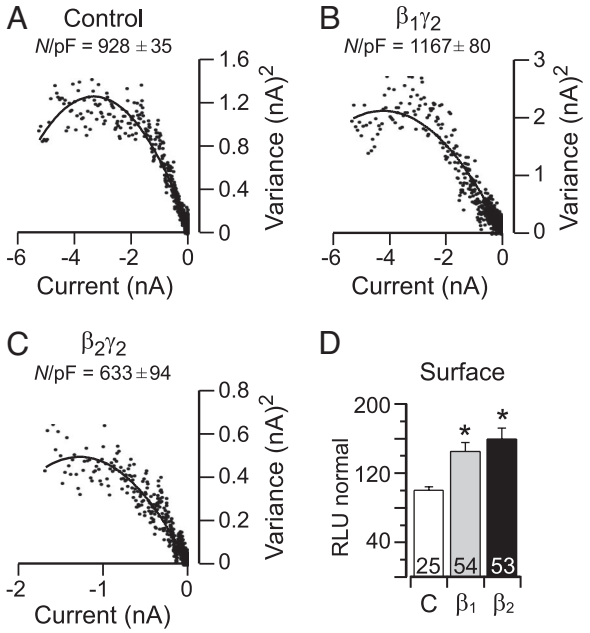

Fig. 2. Gβ_1 and Gβ_2 increase surface channel expression, but only Gβ_2 reduces active channel number. (*A–C*) Variance analysis of I_{Ca} whole-cell currents. Tail currents were elicited from HEK-293 α_{1H}-stable cells coexpressing GFP and empty vector (pcDNA3) or GFP, Gγ_2, and either wild-type Gβ_2 or Gβ_1 by repolarization to −70 mV after repetitive (50 times for 6 sec) test pulses to +30 mV (6 ms), from −90 mV. Shown are variance versus current plots fitted to the function $\sigma^2 = i\ I(t) - I(t)^2/N$ (solid line). Superimposed is the mean number of active channels in the patch (*N/pF*). Notably, the number of active channels (*N/pF*) was increased with G$\beta_1\gamma_2$ expression but reduced with G$\beta_2\gamma_2$ expression compared with control (each $n = 4$, $P < 0.05$). Values for unitary current (*i*) and P_o^{max} were unchanged in each condition: control ($i = 0.73 \pm 0.06$ pA, $P_o^{max} = 0.57 \pm 0.03$, $n = 4$), G$\beta_2\gamma_2$ ($i = 0.81 \pm 0.04$ pA, $P_o^{max} = 0.60 \pm 0.03$, $n = 4$), Gβ_1 ($i = 0.82 \pm 0.06$ pA, $P_o^{max} = 0.62 \pm 0.05$, $n = 4$). (*D*) Quantification of the expressed levels of HA-tagged α_{1H} channels by luminometry. Chemiluminescence from fixed TSA201 cells coexpressing HA-tagged α_{1H} channels, Gγ_2, and either empty vector Gβ_1 or Gβ_2 subunits. Intensity of photon emission is expressed as relative light units (RLU). The histogram plots values for α_{1H} surface expression. Numbers indicate individual cells studied for each condition. *, $P < 0.05$ compares control with treatment groups by ANOVA.

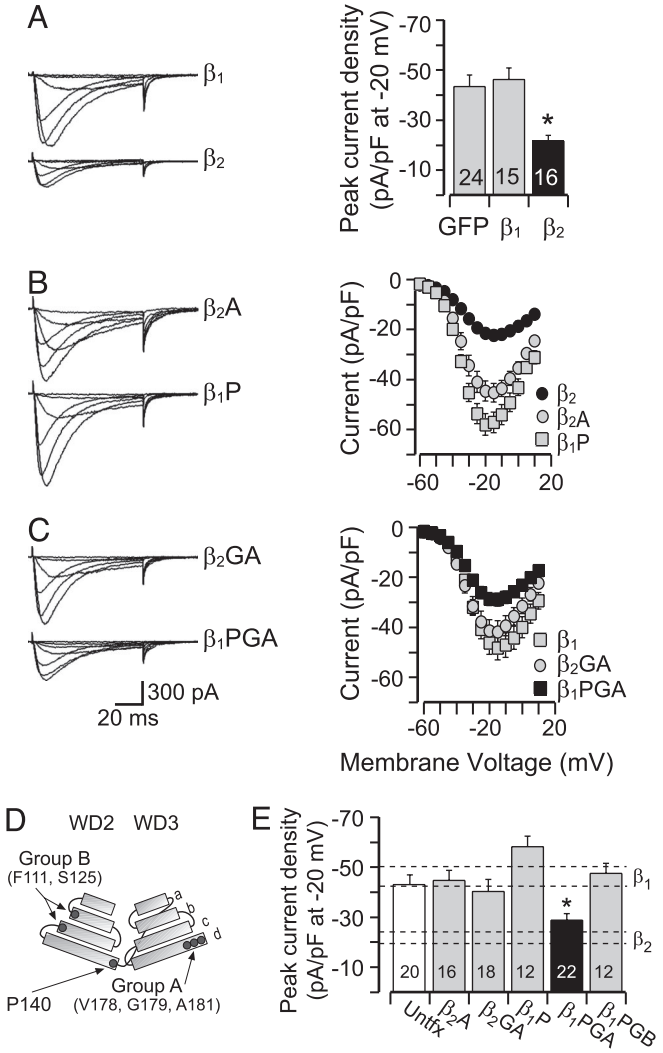

Fig. 3. Four residues are critical for Gβ_2-mediated inhibition of α_{1H} channels. Shown are records from HEK-293 α_{1H}-stable cells expressing various G$\beta_x\gamma_2$ dimers and analysis of I_{Ca} whole-cell currents. (*A–C Left*) Family of sample currents recorded at Vm = −60, −50, −40, −20, −5, and +10 mV (from V_{hold} −90 mV) from cells coexpressing GFP and Gγ_2 and either wild-type Gβ_x (*A*) or mutant Gβ_x proteins β_2A(P140A), β_1P(A140P) (*B*); β_2GA(V178S, G179S, A181S), β_1PGA(A140P, S178V, S179G, S181A) (*C*). (*A–C Right*) (*A*) Histogram plots mean ± SEM of peak current density (pA/pF) obtained from full current–voltage relationships (*I–V*). (*B* and *C*) Maximal current at each test depolarization plotted to construct *I–V* relationships for cells expressing wild-type or mutant G$\beta\gamma$ dimers. Current amplitude is expressed as pA/pF to correct for differences in cell size. (*D*) Schematic model of WD2 and WD3, each showing β-strands (a–d) from Gβ_2. Locations of amino acids selected for mutation are indicated: Group A (GA), Group B (GB), and residue 140. (*E*) Mean current density (±SEM) at −20 mV (*I–V* peak) is plotted for each G$\beta_x\gamma_2$ construct. Dashed lines denote I-V peak (mean ± SEM) for wild-type Gβ_2- or Gβ_1-expressing cells for comparison. Numbers indicate cells recorded for each condition. *, $P < 0.05$ compares untransfected (untfx) peak current density with that of G$\beta_x\gamma_2$-expressing cells by ANOVA.

identified the top and side of the β-torus as surfaces for interaction with specific effectors, such as adenylyl cyclase, phospholipase C-β, and several ion channels (13). Interestingly, these same surfaces also mediate the inactivation of the Gα subunit as it reassembles into the α:$\beta\gamma$ heterotrimer (13, 23).

To identify a nonhomologous set of residues in Gβ_2 that could determine the observed specificity of G$\beta\gamma$ action, we mutated candidate residues that were unique to Gβ_2 and predicted to be surface-exposed based on the crystal structure of bovine Gβ_1. We selected P140 (human β_2 sequence), positioned at the end of the outermost d-strand of blade 2 in Gβ_2, and residues sited on the d-strand of blade 3 (Group A: V178, G179, A181) or on the b- and c-strands of blade 2 (Group B: F111, S125). Together, these solvent-exposed amino acids cluster to form distinct domains on the surface of the Gβ protein (Fig. 3*D* and Fig. 6, which is published as supporting information on the PNAS web site) and, thus, could form interaction sites that functionally distinguish Gβ_1 from Gβ_2.

Consistent with observations (9), the selective overexpression of Gβ_2-containing dimers in HEK-293 cells expressing α_{1H} channels decreased whole-cell current at all voltages, reducing peak current density to 50.1 ± 12.4% of that recorded from cells expressing GFP alone (Fig. 3*A*). Mutation of P140 in Gβ_2 to the corresponding residue in Gβ_1 (P140A) restored current density to levels that were indistinguishable from cells expressing Gβ_1 dimers (Fig. 3 *B* and *E*). However, the reciprocal mutation in Gβ_1 (A140P) did not confer current inhibition. We hypothesized that a spatially contiguous region on Gβ_2, the d-strand of blade 3, may also be required for channel-modulatory activity. Indeed, mutagenesis of the selected Group A residues on Gβ_2 to the corresponding residues in Gβ_1 (V178T, G179T, and A181T) restored current density to levels recorded in GFP-transfected or untransfected cells (Gβ_2GA; Fig. 3 *C* and *E*). Because the

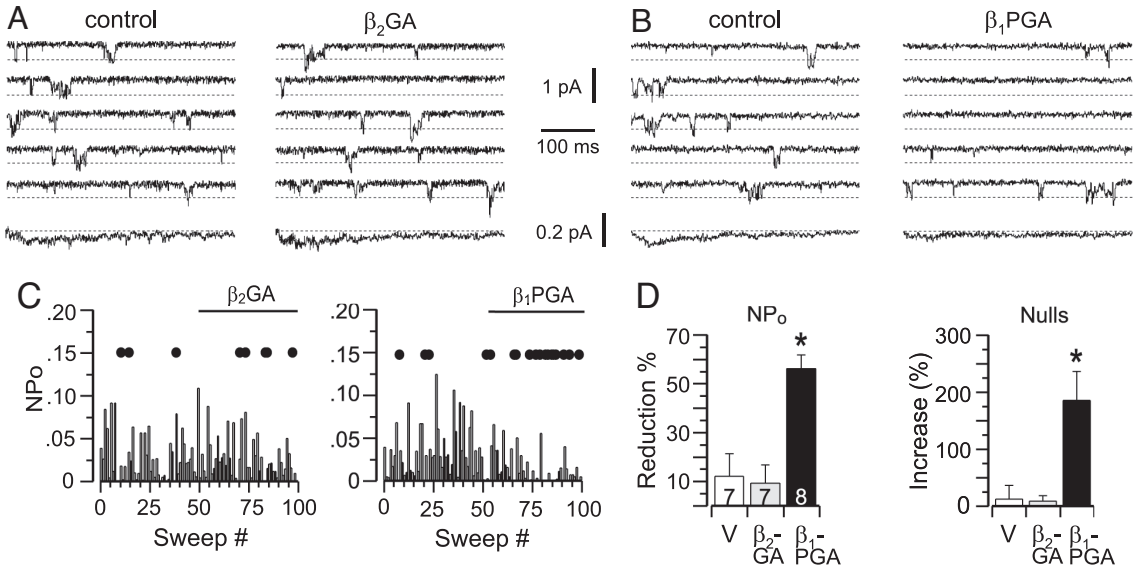

Fig. 4. After residue swapping, recombinant $G\beta_1PGA\gamma_2$, but not $G\beta_2GA\gamma_2$, inhibits α_{1H} channel activity in the excised patch. Shown are records and analysis of single-channel I_{Ca} currents elicited by repeated (6-sec) test pulses to −35 mV from −90 mV (*Methods*). (*A* and *B*) Five consecutive sweeps and the ensemble average of 105 sweeps concatenated from three cells (bottom trace) recorded before (*Left*) and after (*Right*) reconstitution of 1 nM recombinant $G\beta_2GA\gamma_2$ (*A*) or $G\beta_1PGA\gamma_2$ (*B*). (*C*) Time course of NP_o from two representative patches. Sequential exposure to vehicle (sweeps 1–50) and in sweeps 51–100 $G\beta_x\gamma_2$ dimer: $G\beta_2GA\gamma_2$ (*Left*) or $G\beta_1PGA\gamma_2$ (*Right*). Blank/inactive sweeps (nulls) are indicated by filled circles arbitrarily drawn at 0.15 (NP_o) for clarity. (*D*) Bar graphs plot mean ± SEM of the percent reduction in NP_o (*Left*) or percent increase in nulls (*Right*) elicited by $G\beta_2GA\gamma_2$ or $G\beta_1PGA\gamma_2$ relative to vehicle exposure for each patch. Numbers indicate patches recorded for each condition. *, $P < 0.05$ compares vehicle with treatment groups by ANOVA.

independent mutagenesis of P140 and Group A residues removed inhibition, we reasoned that, together, these residues might define a region critical for α_{1H} channel interaction. In combination with the mutagenesis of A140P, the reciprocal mutation of Group A residues in $G\beta_1$ conferred channel-inhibitory activity to $G\beta_1$ ($G\beta_1PGA$; Fig. 3 *C* and *E*) that notably was identical to that of wild-type $G\beta_2$. Moreover, this set of residues (P140, V178, G179, and A181) produced a channel-inhibitory activity in $G\beta_1$ that was not mimicked by the $G\beta_1PGB$ mutant (A140P, Y111F, and N125S), highlighting the specificity of the identified region for channel-inhibitory interactions (Fig. 3*E*).

Because all $G\beta_{(1-4)}\gamma_x$ subunits stimulate GIRK1,4 channel activity (13, 14), we tested each mutant in a GIRK1,4 whole-cell channel assay to confirm activity. As expected, both $G\beta_1$- and $G\beta_2$-containing dimers increased the conductance of GIRK channels equivalently, eliciting an ≈4-fold stimulation that was mimicked by $G\beta$ mutants that either lacked or possessed α_{1H} channel-inhibitory activity (Fig. 7, which is published as supporting information on the PNAS web site). Thus, residue swapping on blades 2 and 3 of $G\beta\gamma$ did not disrupt GIRK-effector contact sites that map to other regions of the $G\beta\gamma$ structure.

Based on our whole-cell studies, we anticipated that the $G\beta_2GA$ mutations would remove $G\beta_2$ activity, and the $G\beta_1PGA$ mutations would confer activity to recombinant proteins tested for direct channel-inhibitory activity. We prepared recombinant $G\beta\gamma$ protein encoding these mutant sequences. Unlike wild-type $G\beta_2$, $G\beta_2GA$ failed to decrease single-channel activity (Fig. 4*A*). Neither the NP_o nor the number of null sweeps was changed within the 5-min recording period by $G\beta_2GA$ added to each of seven patches (Fig. 4 *A*, *C*, and *D*). By contrast, $G\beta_1PGA$ consistently and significantly reduced the single-channel open probability, decreasing NP_o by 56 ± 6% and concomitantly increased the number of silent sweeps by 186 ± 50% (Fig. 4 *B–D*). These changes in single-channel activity fully replicate the inhibitory activity of wild-type $G\beta_2$. Thus, candidate sites identified in our whole-cell studies provide the molecular basis for $G\beta_2$ inhibitory activity.

Discussion

It is now well established that ion channels are direct downstream targets of $G\beta\gamma$ dimers. $G\beta\gamma$ dimers increase GIRK K^+ currents (13, 14) and persistent Na^+ currents (24) and inhibit high-voltage-activated Ca^{2+} currents carried by N-, P/Q- and R-type Ca^{2+} channels (19, 25). We show here that the inhibition of α_{1H} channels also depends on a direct $G\beta\gamma$–channel interaction. Only the dimeric isoform that binds to the II-III loop of α_{1H} channels, $G\beta_2\gamma_2$, inhibits α_{1H} unitary current in the excised patch, and $\alpha_{1H}(G_{II-III})$ chimeric channels, to which $G\beta_2\gamma_2$ cannot bind, are not inhibited by $G\beta_2\gamma_2$. However, even though this inhibition is membrane-delimited, $G\beta_2\gamma_2$ neither slows the kinetics of channel opening to prolong the latency to first opening nor shifts the voltage-dependence of channel activation. Moreover, inhibition cannot be temporarily relieved by a strong depolarizing prepulse. Thus, the inhibition of α_{1H} channels does not possess the hallmarks of voltage-dependent inhibition of N- and P/Q-type channels transduced by $G\beta\gamma$ dimers (15, 25).

On the other hand, voltage-independent (VI) inhibition of high-voltage-activated (HVA) channels manifests as a scaled reduction in steady-state current (26) that is not reversed by prepulse (27, 28). VI inhibition does not rely on a direct $G\beta\gamma$-channel interaction but, rather, may be the result of either second-messenger-induced phosphorylation and internalization of the channel pore protein (28–30) or the depletion of membrane acidic phosphoinositides ($PtdIns(4,5)P_2$) (26, 31) that destabilizes channel activity. Here, we show that, although $G\beta_2\gamma_2$ effects a scaled reduction in current and reduces the number of functional channels, α_{1H} channels are not removed from the plasma membrane, and channel activity is not destabilized in the excised patch configuration, even with Ca^{2+} chelation. Thus, from our experiments, we conclude that the inhibition of α_{1H} channels by $G\beta_2\gamma_2$ defines a unique inhibitory behavior.

Our experiments also identify a cluster of 4 aa (P140, V178, G179, and A181) that can account for the specificity of $G\beta_2\gamma_2$ action on α_{1H} channels. The loss of function upon removal of these residues from $G\beta_2$ and the complementary gain of function upon their transfer to $G\beta_1$ argues strongly that these residues, located on the outermost strand of blades 2 and 3, are essential for the interaction of $G\beta_2$-containing dimers with α_{1H} channels. By contrast, multiple effector-binding regions on the β-torus have been found to be important for regulating HVA channel activity. Early mutagenesis studies identified residues that cluster on the top surface of the β-torus and along the side of blade 1 within a binding surface shared by the GDP-bound form of the α-subunit (32). However, other regions that lie opposite to the $G\alpha$-interaction surface, containing critical residues Y111 and S189, also have been identified for their importance in $G\beta\gamma$ subtype-selective potency (33, 34). Nonetheless, these regions are not sufficient to confer inhibitory activity to inactive rat $G\beta_5$, suggesting additional critical N-type Ca^{2+} channel-interacting sites remain to be identified (33). On the other hand, the C-terminal 25 aa of the β-torus can confer full $G\beta\gamma$ regulation to both P/Q-type Ca^{2+} channels and GIRK K^+ channels, suggesting that blades 6 and 7 may form a common binding surface on the β-torus for these effectors (35).

Specificity in $G\beta\gamma$ signaling typically is achieved by coupling specific heterotrimeric G proteins to distinct types of receptors (36) and by unique responses among effector isotypes (36, 37). Our data indicate that specificity can also be determined by unique effector contact sites on the surface of the β-torus. We have identified a set of residues on $G\beta_2$ that can account for its differential regulation of α_{1H} channel activity. These residues may not be the only sites of effector contact with α_{1H} channels, because other residues conserved across all $G\beta\gamma$ subtypes may also be important structural determinants. Nevertheless, our studies show that $G\beta\gamma$ subtype-selective activity can be determined by a few residues. This mode of selectivity allows $G\beta\gamma$ the choice of effector for the transmission of its signal and raises the possibility that, in the dorsal root ganglion, LVA Ca^{2+} channels are chosen for inhibition by $G\beta_2$.

Methods

Cell Culture and Transfection. HEK-293 cells stably expressing α_{1H} channels were cultured (9) and transiently cotransfected with plasmids for GFP/$G\gamma_2$/$G\beta_x$ in a ratio of 1:6:6 μg by using $CaPO_4$ as reported (9). Cells were cultured 2 days before overnight plating for electrophysiological recording made 72 h after transfection (9).

Molecular Biology. The residue 140, Group A, and Group B mutations were introduced by using the QuikChange XL Site-Directed Mutagenesis kit (Stratagene, La Jolla, CA) (see *Supporting Methods*, which is published as supporting information on the PNAS web site, for primer sequences). All mutations were confirmed by sequencing (University of Virginia Sequencing Facility), and coding regions were excised (BamH1/XhoI) and subcloned into the mammalian expression vector pcDNA3.1.

Generation of Recombinant $G\beta_x\gamma_2$. The coding regions from all wild-type and mutant $G\beta_1$ or $G\beta_2$ constructs (Guthrie Research Institute, Sayre, PA) were excised from pcDNA3.1 by BamH1/XbaI restriction digest and subcloned into pVL1393 baculovirus transfer vector (BD Biosciences/Pharmingen, San Diego, CA). Constructs were validated by restriction enzyme digest, fragment analysis, and sequencing. Recombinant $G\beta_x$ baculoviruses were generated in Sf9 insect cells by using the BaculoGold system (BD Biosciences/Pharmingen), plaque purified, and a high-titer stock prepared (36). Sf9 cells were infected at a MOI of 3 with high-titer virus encoding for a $[His]_6$-tagged $G\alpha_{i1}$ and the desired $G\beta_x$ and $G\gamma_2$ subunits, cell membranes prepared, and the extracts applied to a Ni^{2+}-NTA column. $G\beta_x\gamma_2$ subunits were eluted from the Ni^{2+}-bound α_i subunit with AlF, ensuring the recovery of correctly folded $G\beta\gamma$ dimers (36). The activity of pure $G\beta\gamma$ dimers was verified by testing for PLC-β activation in synthetic lipid vesicles (37).

Electrophysiology. HEK-293 cells were recorded as described by using an Axopatch 200A amplifier, and data were collected with PCLAMP 9.2 software.

Single-channel. Currents from inside-out excised patches were elicited by a test pulse to -35 or -40 mV from -90 mV (200 msec, 6-sec interpulse) (38). Currents were filtered at 2 kHz and sampled at 100 kHz. The external (pipette) solution was 75 mM CsCl, 60 mM $CaCl_2$, and 10 mM Hepes, pH 7.4 (with CsOH). The bath solution was 140 mM potassium-aspartate, 5 mM $MgCl_2$, 10 mM EGTA, 20 mM Hepes, pH 7.4 (with KOH), 0.162 mM CHAPS (0.01%), and 0.04 mM DTT. Purified $G\beta\gamma$ subunits were diluted in bath solution. At the end of each recording, the exact $G\beta\gamma$ concentration (1–20 nM) was determined from the measured bath volume. Analysis of single-channel records was performed by using Clampfit 9.2 (Axon Instruments/Molecular Devices, Sunnyvale, CA) using the 50% threshold crossing criterion for event detection (further details in *Supporting Methods*).

Whole-cell. Currents were elicited as described (9). The internal (pipette) solution was 115 mM CsCl, 1 mM TBACl, 1 mM $MgCl_2$, 5 mM Mg-ATP, 1 mM Li-GTP, 20 mM Hepes, pH 7.2 (with CsOH), and 11 mM BAPTA; added $CaCl_2$ fixed free Ca^{2+} at 27 nM (0.9 mM). The bath solution was 127 mM TEACl, 10 mM $CaCl_2$, 0.5 mM $MgCl_2$, 10 mM Hepes, 5 mM dextrose, and 32 mM sucrose, pH 7.4 (with CsOH). Currents were filtered at 2 kHz and sampled at 12.5 kHz, and leak subtraction was performed on line by using scaled hyperpolarizing steps of one-fourth amplitude (P/N4). ANOVA was used for statistical examination with post hoc Dunnett's test, where significance was taken as $P < 0.05$. Data are given as mean ± SEM.

Noise analysis. Tail currents were elicited by -70 mV after repetitive (6-sec) test pulses (6 msec, +30 mV, from -90 mV) from HEK-293 cells stably expressing α_{1H} channels. The internal (pipette) solution was identical to that described above for whole-cell recording. Bath solution replaced Ca with Ba to reduce charge screening: 117 mM TEACl, 20 mM $BaCl_2$, 0.5 mM $MgCl_2$, 10 mM Hepes, 5 mM dextrose, and 32 mM sucrose, pH 7.4 (adjusted with CsOH). Currents were filtered at 5 kHz and sampled at 25 kHz; leak subtraction was performed on line by using scaled hyperpolarizing steps of one-fourth amplitude (P/N4). ANOVA was used for statistical examination with post hoc Dunnett's test, where significance was taken as $P < 0.05$.

Nonstationary Noise (Variance) Analysis. Briefly, $[I(t)]$ for each isochrone was used to compute the experimental nonstationary ensemble variance. To correct for basal noise, the average variance at -90 mV was subtracted from that obtained during the test pulse. The subtracted variance (σ^2) of the tail current (-70 mV) was plotted versus the mean current and the data fitted to (20) $\sigma^2 = iI(t) - I(t)^2/N$, where i = single-channel current amplitude, and N = number of active channels. i was obtained from the initial slope and N from nonlinear curve-fitting analysis performed using Origin (OriginLab, Northampton, MA). The maximum open probability, P_o^{max}, was obtained from the relationship: $P_o^{max} = I_{max}/iN$, where I_{max} is the maximum mean current measured in the experiment.

Surface Expression Measurements. TSA201 cells cultured in 24-well plates were transiently transfected by using Fugene 6 (Roche, Basel, Switzerland) with plasmids for α_{1H}-HA, ($Ca_v3.2$-HA-GFP-pEGFP-C), $G\gamma_2$, and either the $G\beta_1$ or $G\beta_2$ at a 1:1:1 ratio (0.5 μg of DNA per well). The culture medium (Invitrogen) was

changed 24 h after transfection and the luminometric assay performed as described (22) on 4% paraformaldehyde-fixed cells. Primary and secondary antibodies used for α_{1H} channel detection were a monoclonal rat anti-HA (clone 3F10; Roche Applied Science) and a horseradish peroxidase (The Jackson Laboratory, Bar Harbor, ME), respectively (further details in *Supporting Methods*). Eleven independent sets of transfections were performed for each condition and results presented as mean ± SEM ($P < 0.05$).

We thank Robert Clay for technical assistance. This work was supported by National Institutes of Health Grants HL36977 (to P.Q.B.) and DK19952 (to J.C.G.). S.D.D. was supported by a predoctoral fellowship from the American Heart Association Mid-Atlantic Affiliate.

1. Perez-Reyes E (2003) *Physiol Rev* 83:117–161.
2. Todorovic SM, Meyenburg A, Jevtovic-Todorovic V (2004) *Pain* 109:328–339.
3. Bourinet E, Alloui A, Monteil A, Barrere C, Couette B, Poirot O, Pages A, McRory J, Snutch TP, Eschalier A, Nargeot J (2005) *EMBO J* 24:315–324.
4. Chen Y, Lu J, Pan H, Zhang Y, Wu H, Xu K, Liu X, Jiang Y, Bao X, Yao Z, *et al.* (2003) *Ann Neurol* 54:239–243.
5. Welsby PJ, Wang H, Wolfe JT, Colbran RJ, Johnson ML, Barrett PQ (2003) *J Neurosci* 23:10116–10121.
6. Fearon IM, Randall AD, Perez-Reyes E, Peers C (2000) *Pflugers Arch Eur J Physiol* 441:181–188.
7. Marchetti C, Carbone E, Lux HD (1986) *Pflugers Arch Eur J Physiol* 406:104–111.
8. Lledo PM, Homburger V, Bockaert J, Vincent JD (1992) *Neuron* 8:455–463.
9. Wolfe JT, Wang H, Howard J, Garrison JC, Barrett PQ (2003) *Nature* 424:209–213.
10. Scott RH, Wootton JF, Dolphin AC (1990) *Neuroscience* 38:285–294.
11. Scott RH, Dolphin AC (1987) *Topics and Perspectives in Adenosine Research, Proceedings of the Third International Adenosine Symposium* (Springer, Munich), pp 549–558.
12. Hildebrandt JD (1997) *Biochem Pharmacol* 54:325–339.
13. Clapham DE, Neer EJ (1997) *Ann Rev Pharmacol Toxicol* 37:167–203.
14. Logothetis DE, Kurachi Y, Galper J, Neer EJ, Clapham DE (1987) *Nature* 325:321–326.
15. Herlitze S, Garcia DE, Mackie K, Hille B, Scheuer T, Catterall WA (1996) *Nature* 380:258–262.
16. Ruiz-Velasco V, Ikeda SR (2000) *J Neurosci* 20:2183–2191.
17. Arnot MI, Stotz SC, Jarvis SE, Zamponi GW (2000) *J Physiol (London)* 527(Pt 2):203–212.
18. Garcia DE, Li B, Garcia-Ferreiro RE, Hernandez-Ochoa EO, Yan K, Gautam N, Catterall WA, Mackie K, Hille B (1998) *J Neurosci* 18:9163–9170.
19. Dolphin AC (2003) *Pharmacol Rev* 55:607–627.
20. Sigworth FJ (1980) *J Physiol (London)* 307:97–129.
21. Alvarez O, Gonzalez C, Latorre R (2002) *Adv Physiol Educ* 26:327–341.
22. Dubel SJ, Altier C, Chaumont S, Lory P, Bourinet E, Nargeot J (2004) *J Biol Chem* 279:29263–29269.
23. Cabrera-Vera TM, Vanhauwe J, Thomas TO, Medkova M, Preininger A, Mazzoni MR, Hamm HE (2003) *Endocr Rev* 24:765–781.
24. Ma JY, Catterall WA, Scheuer T (1997) *Neuron* 19:443–452.
25. Zamponi GW, Snutch TP (1998) *Curr Opin Neurobiol* 8:351–356.
26. Wu L, Bauer CS, Zhen XG, Xie C, Yang J (2002) *Nature* 419:947–952.
27. Diverse-Pierluissi M, Dunlap K (1993) *Neuron* 10:753–760.
28. Diverse-Pierluissi M, Remmers AE, Neubig RR, Dunlap K (1997) *Proc Natl Acad Sci USA* 94:5417–5421.
29. Tombler E, Cabanilla NJ, Carman P, Permaul N, Hall JJ, Richman RW, Lee J, Rodriguez J, Felsenfeld DP, Hennigan RF, Diverse-Pierluissi MA (2006) *J Biol Chem* 281:1827–1839.
30. Altier C, Khosravani H, Evans RM, Hameed S, Peloquin JB, Vartian BA, Chen L, Beedle AM, Ferguson SS, Mezghrani A, *et al.* (2006) *Nat Neurosci* 9:31–40.
31. Gamper N, Reznikov V, Yamada Y, Yang J, Shapiro MS (2004) *J Neurosci* 24:10980–10992.
32. Ford CE, Skiba NP, Bae H, Daaka Y, Reuveny E, Shekter LR, Rosal R, Weng G, Yang CS, Iyengar R, *et al.* (1998) *Science* 280:1271–1274.
33. Doering CJ, Kisilevsky AE, Feng ZP, Arnot MI, Peloquin J, Hamid J, Barr W, Nirdosh A, Simms B, Winkfein RJ, Zamponi GW (2004) *J Biol Chem* 279:29709–20717.
34. Tedford HW, Kisilevsky AE, Peloquin JB, Zamponi GW (2006) *J Neurophysiol* 96:465–470.
35. Li X, Hummer A, Han J, Xie M, Melnik-Martinez K, Moreno RL, Buck M, Mark MD, Herlitze S (2005) *J Biol Chem* 280:23945–23959.
36. McIntire WE, MacCleery G, Garrison JC (2001) *J Biol Chem* 276:15801–15809.
37. Myung CS, Yasuda H, Liu WW, Harden TK, Garrison JC (1999) *J Biol Chem* 274:16595–16603.
38. Barrett PQ, Lu HK, Colbran R, Czernik A, Pancrazio JJ (2000) *Am J Physiol* 279:C1694–C1703.